Proceedings of the XXX International School of Semiconducting Compounds, Jaszowiec 2001

Quantum States of Self-Assembled InAs Dots Probed by Magneto-Tunneling Spectroscopy

A. Patanè, L. Eaves, P.C. Main, A. Levin, M.L. Zambrano, M. Henini

School of Physics and Astronomy, University of Nottingham
Nottingham NG7 2RD, UK

E.E. Vdovin, Y.V. Dubrovskii

Institute of Microelectronics Technology, RAS, 142432 Chernogolovka, Russia

and G. Hill

Dept. of Electronic and Electrical Engineering, University of Sheffield
S3 3JD Sheffield, UK

We present an experimental study of the electron wave function in InAs/GaAs self-assembled quantum dots. Magneto-tunneling spectroscopy is employed as a non-invasive probe to produce two-dimensional images of the probability density of an electron confined in a quantum dot. The images reveal the elliptical symmetry of the ground state and the characteristic lobes of the higher energy states of the dots.

PACS numbers: 73.63.–b, 73.63.Kv, 73.43.Jn

1. Introduction

During the last few years there has been continuous and increasing interest in imaging the quantum environment of electrons and atoms. In particular, various scanning probe techniques, such as the scanning tunneling microscopy (STM) [1–3] and scanning single-electron transistor microscopy (SETM) [4, 5] have been successfully used to probe atoms or electron charge distributions in a wide variety of systems, including metals and superconductor materials. This raises the question

of whether it is now possible to image the electron wave function in a quantum dot (QD), an artificial nanometre-sized cluster, which confines the motion of an electron in all three spatial dimensions [6]. In a QD, electrons are confined to length scales of $\approx$ 10 nm and their behavior is characterized by quantum mechanical effects, such as a discretization of the energy levels, similar to that in atoms.

In principle, it is possible to investigate the probability density of electrons in a QD using surface probe techniques such as STM. However, although STM is a powerful tool for imaging the electronic states of dots lying on a surface, a different technique is required for dots incorporated in real semiconductor devices, where the dots may be buried hundreds of nanometers below the surface. The imaging of the wave function of a QD was reported in a recent paper [7]: cross-sectional STM (XSTM) of cleaved InAs/GaAs self-assembled QDs was used to probe the profile of the electron density along the plane of vertical confinement of the dot (i.e. along the growth direction and one-in plane direction). However, since the probed wave patterns arose from a superposition of the probability densities of the electron ground and excited states, the technique did not allow the various confined states of the dot to be distinguished. This paper describes how magneto-tunneling spectroscopy (MTS) can be used as a non-invasive and non-destructive probe to obtain full maps of the wave function of the ground and excited states of electrons in a QD.

2. Samples

The layer composition and band diagram of our devices are shown schematically in Fig. 1. A layer of InAs self-assembled QDs is embedded in the centre of an undoped 12 nm GaAs quantum well (QW), which is sandwiched between two 8.3 nm $Al_{0.4}Ga_{0.6}As$ tunnel barriers. The layer of InAs QDs was grown by depositing 2.3 monolayers (ML) of InAs. Undoped GaAs spacer layers of width 50 nm separate the barriers from two contact layers with graded n-type doping [8]. The device acts as a resonant tunneling diode in which electrons can tunnel into the QD from a doped contact layer on the opposite side of the barrier. Here we focus on two structures, labelled A1 and A2, grown respectively on a (311)B- and a (100)-oriented GaAs substrate. For comparison, we have also studied a series of control samples: two samples were grown with the same sequence of layers, except one has only a thin InAs two-dimensional wetting layer (i.e. containing no QDs) and the other has no InAs layer at all; the second control sample is an $Al_{0.4}Ga_{0.6}As/GaAs/Al_{0.4}Ga_{0.6}As$ tunneling diode in which the central plane of the quantum well was lightly doped with 4×10^9 cm^{-2} Si donors [9].

The layer of InAs QDs introduces a set of discrete electronic states below the GaAs conduction band edge. At zero bias, equilibrium is established by some electrons diffusing from the doped GaAs layers into the dot states. The resulting negative charge in the QW produces depletion layers in the region beyond the

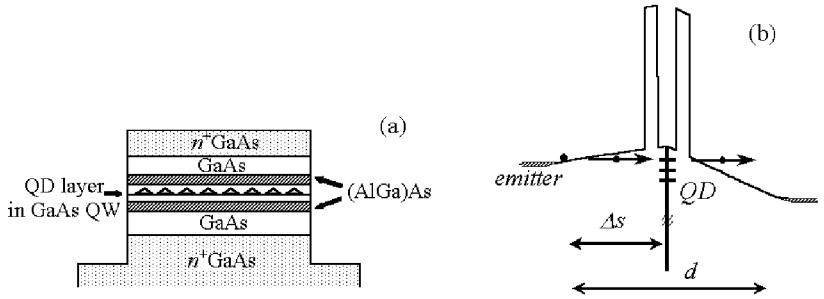

Fig. 1. (a) Schematic diagram of a $n-i-n$ GaAs/(AlGa)As tunneling diode incorporating a layer of quantum dots in the centre of the GaAs well. (b) Schematic conduction band profile under an applied bias of the device shown in (a). Δs is the tunneling distance from the emitter to the QD layer.

(AlGa)As barrier. When a voltage, V, is applied, resonant tunneling through a particular QD state leads to a resonance in the current–voltage, $I(V)$, plot whenever the energy of the state is resonant with an adjacent filled state in the negatively biased electron emitter layer.

3. Experimental results and discussion

Figure 2 shows the low-temperature ($T = 4.2$ K) $I(V)$ characteristics in reverse bias (positive biased substrate) in the presence of a magnetic field, B, applied parallel to the growth plane (x, y) for sample A1. A series of resonant features labelled e_1-e_7 are observed. The resonant peaks are not observed in samples with no dots, so they are related directly to the presence of the InAs QD layer.

For each resonant feature, we observe a thermally-activated current onset, which is an unambiguous signature of an electron tunneling from a thermalized Fermi-distribution of emitter states into an individual, discrete and sharp QD energy level [10]. Previous tunnel current measurements at low temperatures on structures containing a large ensemble of quantum dots have also revealed the presence of resonant tunneling peaks due to individual dots in the range of bias close to the threshold of current flow [10–14].

The amplitude of each resonance exhibits a strong dependence on the intensity of B. In particular, we can identify three characteristics types of magnetic field dependence: type I (peaks e_1, e_2, e_3) shows a maximum in I at $B = 0$ T followed by an almost monotonic decay to zero at around 8 T; type II (e_4 and e_5) shows a broad maximum in I at ≈ 4 T, followed by a gradual decay to zero; type III (e_6 and e_7) shows two clear maxima in I at $B = 0$ T and ≈ 5 T, with I falling to a minimum value of almost zero between these maxima.

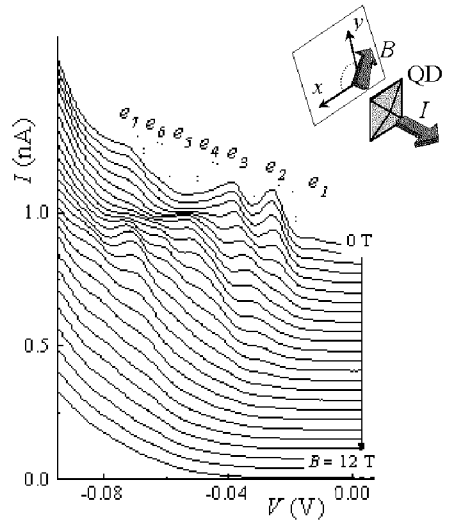

Fig. 2. Low-temperature ($T = 4.2$ K) $I(V)$ characteristics in reverse bias (positive biased substrate) in the presence of a magnetic field, B, perpendicular to the current for sample A1. B is increased in steps of 0.5 T and the corresponding curves are displaced along the current axis for clarity. The inset sketches the geometry of our magneto-tunneling experiment.

We can understand the magnetic field dependence of the resonances in terms of the effect of B on a tunneling electron. Let α, β, and z indicate, respectively, the direction of B, the direction normal to B in the growth plane (x, y), and the normal to the tunnel barrier, respectively. When an electron tunnels from the emitter into the dot, it acquires an additional in-plane momentum given by [15]:

$$k_\beta = eB\Delta s/\hbar, \tag{1}$$

where Δs is the effective distance tunneled along z. This effect can be understood semiclassically in terms of the increased momentum along β, which is acquired by the tunneling electron due to the action of the Lorentz force. The applied voltage allows us to tune resonantly to the energy of a particular QD state. Then, by measuring the variation of the tunnel current with B, we can determine the size of the matrix element that governs the quantum transition of an electron as it tunnels from a state in the emitter layer into a QD. In our experiment, the tunneling matrix element is most conveniently expressed in terms of the Fourier transforms $\varphi_{\mathrm{i(f)}}(k)$ of the conventional real space wave functions [16]. Here the subscripts i and f indicate the initial (emitter) and final (QD) states of the tunnel transition. Relative to the strong spatial confinement in the QD, the initial state in the emitter has only weak spatial confinement. Hence, in k-space $\varphi_{\mathrm{i}}(k)$ corresponds to a sharply peaked function with a finite value centred around $k = 0$. Since the tunnel current is given by the square of the matrix element involving $\varphi_{\mathrm{i}}(k)$ and

$\varphi_{\rm f}(k)$, the narrow spread of k for $\varphi_{\rm i}(k)$ allows us to determine the form of $\varphi_{\rm f}(k)$ by varying B and hence k. Thus by plotting $I(B)$ for a *particular* direction of B we can measure the dependence of $|\varphi_{\rm QD}(k)|^2$ along the k-direction perpendicular to B. Then, by rotating B in the plane (x, y) and making a series of measurements of $I(B)$ with B set at regular intervals of the rotation angle, we obtain a full spatial profile of $|\varphi_{\rm QD}(k_x, k_y)|^2$. This represents the projection in k-space of the probability density of a given electronic state confined in the QD [17].

Figure 3 shows the form of the differential conductance $G(B) = {\rm d}I/{\rm d}V \sim |\varphi_{\rm QD}(k_x, k_y)|^2$, in the plane $(k_x,\ k_y)$ for three representative QD states, corresponding to the resonances e_2, e_4, and e_7 in Fig. 2. We use $G(B)$ plots rather than $I(B)$ plots since the differential conductance allows us to identify the onset of the resonance due to each QD and to determine more clearly the magnetic field dependence of each resonant feature. The contour plots reveal clearly the characteristic form of the probability density distribution of a ground state orbital (e_2) and the characteristic lobes of the higher energy states (e_4 and e_7) of the QD.

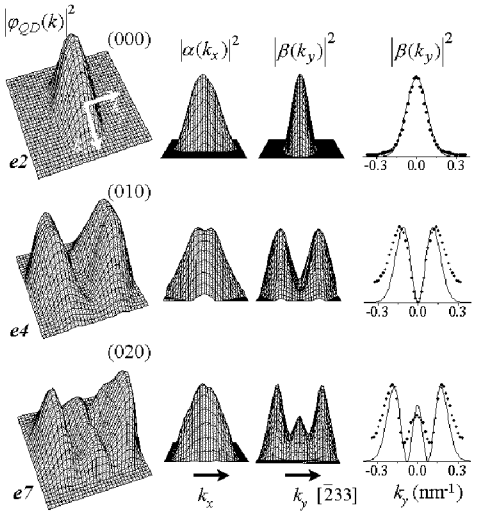

Fig. 3. Distribution in the plane (k_x, k_y) of the differential conductance, G, for three representative states, (000), (010), and (020), of quantum dots grown on a (311)B-oriented GaAs substrate (sample A1). This provides a spatial map of $|\varphi_{\rm QD}(k_x, k_y)|^2$, the probability density in k-space of an electron confined in the dot. The form of $|\varphi_{\rm QD}(k_x, k_y)|^2$ along k_x ($|\alpha(k_x)|^2$) and k_y ($|\beta(k_y)|^2$) is also shown in the inset. Continuous lines show the wave function probability in k- and real-space for the three lowest energy states of a harmonic oscillator with parameters determined by a fit to the $|\beta(k_y)|^2$ data (full circles). The value of k_y is determined according to the relation $k_y/B = e\Delta s/\hbar = 3 \times 10^7$ m^{-1} T^{-1}, where Δs is the tunneling distance (≈ 20 nm).

It is clear from Fig. 3 that $|\varphi_{\mathrm{QD}}(k_x)|^2$ has approximately the same form for all three states, whereas $|\varphi_{\mathrm{QD}}(k_y)|^2$ corresponds to the lower states of quantization along y and has similar form to that of the ground and first and second excited states of a simple harmonic oscillator. This suggests that, to a reasonable approximation, the probability density in k-space, $|\varphi_{\mathrm{QD}}(k_x, k_y)|^2$, is separable, i.e. $|\varphi_{\mathrm{QD}}(k_x, k_y)|^2 = |\alpha(k_x)|^2 \, |\beta(k_y)|^2$. Although our measurements reveal detailed information about the symmetry of the QD wave functions with respect to the in-plane coordinates, they give us no information about the z-dependence. This is directly related to the morphology of the QDs: in general, the dot height is much smaller than the dimensions of the base. Therefore, the quantization energy of confinement along z is much higher than that for in-plane motion. In our discussion of the magneto-tunneling data we have made two reasonable assumptions. The first is that the motion along z is separable from the in-plane motion. Our second assumption is that all the observed peaks involve final QD states that share the same type of quantum confinement along z. This approximation allows us to label the QD state using quantum numbers for the in-plane motion and for motion along z and to assign quantum numbers $(n_x, n_y, n_z) = (000), (010)$, and (020) to the states shown in Fig. 3.

The contour plots of $|\varphi_{\mathrm{QD}}(k_x, k_y)|^2$ reveal that the electron wave function has a biaxial symmetry in the growth plane, with axes corresponding quite closely to the main crystallographic directions $[01\bar{1}]$ and $[\bar{2}33]$ on the (311)B plane (see Figs. 3 and 4a). The probability density in k-space is narrower along the $[\bar{2}33]$ direction (see Fig. 3). This indicates that the wave function probability densities in real space is elongated along this direction and suggests that the dot shape is not isotropic. Consistently, the characteristic lobes of the first and second excited state are aligned along the elongated base of the dot. The in-plane anisotropy of the electron wave function is less pronounced for InAs QDs grown on a (100)-oriented GaAs substrate (sample A2). Figure 4b shows a plot of $|\varphi_{\mathrm{QD}}(k_x, k_y)|^2$ in the plane (k_x, k_y) for the ground state of (100) QDs. The wave function has a biaxial symmetry in the growth plane, with axes corresponding quite closely to two main crystallographic axes, x and y ([010] and [001] axes). The wave function is elongated along one crystallographic axis, but the anisotropic effects are less pronounced than in the case of (311)B QDs. For the excited state, the wave function exhibits a central node and characteristics lobes, which are not as clearly oriented as for the (311)B QDs. The different form of the excited state may originate from the different shapes of the two types of dots. The anisotropic shape of the (311)B dot leads to a preferential electron distribution along the elongated axis of the dot. In contrast, the more isotropic shape of the (100) dot leads to an almost torus-like distribution of the electron charge.

For comparison purposes and as a means of validating the technique, we have also studied the form of the electron wave function for a hydrogenic-donor impurity state. We used an (AlGa)As/GaAs/(AlGa)As resonant tunneling diode

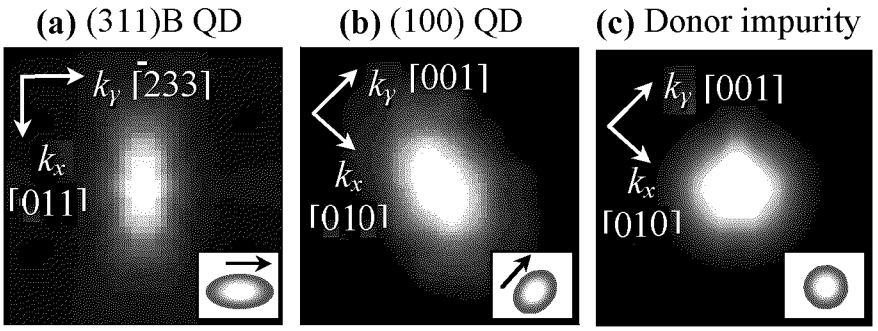

Fig. 4. Distribution in the plane (k_x, k_y) of the probability density of the electron wave function for quantum dots grown on a (311)B- (a) and (100)- (b) oriented GaAs substrate and for donor impurities (c). The arrows indicate two main crystallographic directions on the (100)- and (311)B-oriented plane. The insets sketch the form of the probability density in real space.

in which the central plane of the quantum well was very lightly doped ($\approx 4 \times 10^9$ cm^{-2}) with Si donors [9]. In this case, it has been shown [9] that an additional resonant peak is observed due to tunneling of electrons from the emitter into the $1s$ ground state of the donor. This peak occurs at a bias close to the threshold for tunneling into the lowest energy subband of the QW. We find that the $G(B)$ plots associated with tunneling into the ground state of the donors reveal that the electron wave function has spherical symmetry in the growth plane, as expected for a $1s$ donor ground state (see Fig. 4c). This provides strong supporting evidence for the anisotropic wave functions of the dots (see Figs. 4a, b) being associated with their anisotropic shape and not with the anisotropy of the tunneling coefficient as caused, for example, by an anisotropic electron effective mass [18].

Although the MTS technique permits us to probe the shape of the electron wave function, the determination of its extent is limited by the uncertainty of the value of the tunneling distance, Δs, the parameter which controls the scale of k-values ($k/B = e\Delta s/\hbar$). The average distance an electron tunnels from the emitter to a QD can be estimated from capacitance–voltage measurements. We model the tunneling diode as a parallel-plate capacitor and express the capacitance as $\varepsilon\varepsilon_0 A/d$, where ε is the permittivity constant of GaAs ($\varepsilon = 12.8$), A is the area of our 100 μm diameter mesa and d is the average separation between the edges of the electron gas distributions in the doped emitter and collector (see Fig. 1b). Using the typical value of the capacitance ($C \approx 16$ pF) measured at low bias (< 0.1 V), we find that $d \approx 56$ nm. In turns, this provides an estimate for Δs, which is equal to $d/2 \approx 28$ nm. However, the tunneling distance may vary in the plane of the barrier due to mesoscopic effects in the emitter and we expect that it is smaller for the dots that generate the strong resonances in the $I(V)$ plot. On

the other hand, since the tunneling distance cannot be smaller than the distance of the dot layer from the barrier ($\approx$ 15 nm), we can assume that Δs is in the range 15–28 nm. This leads to an uncertainty in the value of k/B, which varies in the range 2–4$\times 10^7$ m^{-1} T^{-1}, and in the corresponding size of the electron wave function, as estimated from the analysis of the $|\varphi_{\rm QD}(k_x, k_y)|^2$ plots.

Our tunnel current measurements provide information on the wave function probability density in k-space and we can determine the form of the corresponding probability densities in real space if we approximate the $|\varphi_{\rm QD}(k_x, k_y)|^2$ plots by simple functions, e.g. the harmonic functions used to describe the form of the $|\beta(k_y)|^2$ plots of Fig. 3. A particularly noteworthy feature of the $|\beta(k_y)|^2$ curves is that they have very similar forms to the probability density in k-space associated with the ground, first, and second excited states of a harmonic oscillator potential. Also, for a harmonic oscillator potential, the k-space and real space wave functions have identical form and for this case we can obtain directly the electron wave function in real space. For the ground state, $|\beta(k_y)|^2$ can be expressed as $\exp(-k_y^2/\sigma_k^2)$, where σ_k is related to the expectation value of y^2 according to the relation $l_y^2 = \langle y^2 \rangle = \sigma_k^{-2}$. We find $l_y \approx 10 \pm 3$ nm, which is larger than the typical in-plane radius of our dots ($\approx$ 6 nm). This suggests that electrons tunnel into the dots with the largest in-plane area. Also, we find that $\langle y^2 \rangle$ increases with the quantum number n_y, which is consistent with the attribution of resonances e_2, e_4, and e_7 to three consecutive eigenstates. A similar analysis for the $|\alpha(k_x)|^2$ plot allows us to determine the characteristic size, $l_x = 5.5 \pm 1.5$ nm, of the electron wave function along x.

4. Conclusions

In conclusion, we have shown that magneto-tunneling spectroscopy provides a means of probing the electron wave function of self-assembled InAs QDs. We identified confined states in the dot showing the elliptical symmetry of the ground state and the characteristics lobes of the excited states. We have also drawn a correlation between the spatial symmetry of the electron wave function and the morphological properties of quantum dots grown on differently oriented GaAs substrates and compared them with the symmetry properties of the electron wave function of an hydrogenic-donor impurity. MTS studies can now be extended to new material systems and novel devices. In principle, the MTS technique can be used to investigate the wave function of the holes or possibly the quantum states associated to many-body particles in the dot. The detailed images of the electron and hole wave functions provided by MTS may have relevance to further investigations of the physics of quantum dots and to the design of future quantum devices.

References

[1] M.F. Crommie, C.P. Lutz, D.M. Eigler, *Nature* **262,** 218 (1993).

[2] J.F. Zheng, J.D. Walker, M.B. Salmeron, E.R. Weber, *Phys. Rev. Lett.* **72,** 1490 (1994).

[3] S.H. Pan, E.W. Hudson, K.M. Lang, H. Eisaki, S. Uchida, J.C. Davis, *Nature* **403,** 746 (2000).

[4] K.L. McCormick, M.T. Woodside, M.H. Mingshaw Wu, P.L. McEuen, C. Duruoz, J.S. Harris, *Phys. Rev. B* **59,** 4654 (1999).

[5] N.B. Zhitenev, T.A. Fulton, A. Yacoby, H.F. Hess, L.N. Pfeiffer, K.W. West, *Nature* **404,** 473 (2000).

[6] D. Bimberg, M. Grundmann, N.N. Ledentsov, *Quantum Dot Heterostructures*, Wiley, New York 1999 and references therein.

[7] B. Grandidier, Y.M. Niquet, B. Legrand, J.P. Nys, C. Priester, D. Stievenard, J.M. Gerard, V. Thierry-Mieg, *Phys. Rev. Lett.* **85,** 1068 (2000).

[8] A. Patanè, A. Polimeni, L. Eaves, P.C. Main, M. Henini, A.E. Belyaev, Yu.V. Dubrovskii, P.N. Brounkov, E.E. Vdovin, Yu.N. Khanin, *Phys. Rev. B* **62,** 13595 (2000).

[9] J.W. Sakai, T.M. Fromhold, P.H. Beton, L. Eaves, M. Henini, P.C. Main, F.W. Sheard, G. Hill, *Phys. Rev. B* **48,** 5664 (1993).

[10] P.C. Main, A.S.G. Thornton, R.J.A. Hill, S.T. Stoddart, T. Ihn, L. Eaves, K.A. Benedict, M. Henini, *Phys. Rev. Lett.* **84,** 729 (2000).

[11] M. Narihiro, G. Yusa, Y. Nakamura, T. Noda, H. Sakaki, *Appl. Phys. Lett.* **70,** 105 (1997).

[12] I.E. Itskevich, T. Ihn, A. Thornton, M. Henini, T.J. Foster, P. Moriarty, A. Nogaret, P.H. Beton, L. Eaves, P.C. Main, *Phys. Rev. B* **54,** 16401 (1996).

[13] T. Suzuki, K. Nomoto, K. Taira, I. Hase, *Jpn. J. Appl. Phys. Part 1* **36,** 1917 (1997).

[14] D.G. Austing, S. Tarucha, P.C. Main, M. Henini, S.T. Stoddart, L. Eaves, *Appl. Phys. Lett.* **75,** 671 (1999).

[15] R.K. Hayden, D.K. Maude, L. Eaves, E.C. Valadares, M. Henini, F.W. Sheard, O.H. Hughes, J.C. Portal, L. Cury, *Phys. Rev. Lett.* **66,** 1749 (1991).

[16] P.H. Beton, J. Wang, N. Mori, L. Eaves, P.C. Main, T.J. Foster, M. Henini, *Phys. Rev. Lett.* **75,** 1996 (1995).

[17] E.E. Vdovin, A. Levin, A. Patanè, L. Eaves, P.C. Main, Yu.N. Khanin, Yu.V. Dubrovskii, M. Henini, G. Hill, *Science* **290,** 124 (2000).

[18] O.H. Hughes, M. Henini, E.S. Alves, M.L. Leadbeater, L. Eaves, M. Davies, M. Heath, *J. Vac. Sci. Technol. B* **7,** 1041 (1989).